RESEARCH PAPER

Heterostructural coaxial nanotubes of CNT@Fe$_2$O$_3$ via atomic layer deposition: effects of surface functionalization and nitrogen-doping

**Xiangbo Meng · Mihnea Ionescu · Mohammad Norouzi Banis ·
Yu Zhong · Hao Liu · Yong Zhang · Shuhui Sun ·
Ruying Li · Xueliang Sun**

Abstract This study attempted to synthesize one-dimensional (1D) coaxial nanotubes of Fe$_2$O$_3$ based on carbon nanotubes (CNT@Fe$_2$O$_3$) via atomic layer deposition (ALD) using ferrocene and oxygen as precursors. Results disclosed that undoped CNTs were suitable for the ALD of Fe$_2$O$_3$ (ALD-Fe$_2$O$_3$) only if they were chemically functionalized, due to their inert surface nature. It was further demonstrated that the effects of both covalent and non-covalent methodologies were limited in functionalizing undoped CNTs, leading to random and non-uniform deposition of Fe$_2$O$_3$. In sharp contrast, it was found that, as an alternative, nitrogen-doped CNTs (N-CNTs) contributed uniform and tunable ALD-Fe$_2$O$_3$, due to their active surface nature induced by incorporated N atoms. Consequently, various 1D heterostructural coaxial nanotubes were obtained with well-controlled growth of Fe$_2$O$_3$ on N-CNTs. For a better understanding, the underlying mechanisms were explored based on different N-doping configurations. In addition, high-resolution transmission electron microscopy and X-ray diffraction jointly demonstrated that as-deposited Fe$_2$O$_3$ is single-phase crystalline α-Fe$_2$O$_3$ (hematite). The as-synthesized heterostructural coaxial nanotubes of CNT@Fe$_2$O$_3$ may find great potential applications in photocatalysis, gas-sensing, and magnetic fields.

Keywords Atomic layer deposition · Iron oxide · Carbon nanotubes · Nitrogen-doping · Coaxial nanostructures · Nanocomposites

Introduction

Since its emergence in the 1970s (Suntola and Antson 1977), atomic layer deposition (ALD) is currently undergoing a renaissance due to its recognized advantages and the demanding needs in scaling complementary metal-oxide-semiconductor (CMOS) devices (Puurunen 2005). By nature, ALD is a surface-controlled process consisting of two sequential self-limiting half-reactions. As a consequence, ALD has tremendous capabilities to provide more advantages over its counterparts such as chemical vapor deposition (CVD) and physical vapor deposition (PVD): thickness control at the atomic level, excellent conformity for complex structures, very good uniformity with large scale of thin films, and very low growth temperature (even down to room temperature) (Kim 2003; Groner et al. 2004; Suntola 1989; van Hemmen et al. 2007). More recently, especially since the very

X. Meng · M. Ionescu · M. N. Banis · Y. Zhong ·
H. Liu · Y. Zhang · S. Sun · R. Li · X. Sun (✉)
Department of Mechanical and Materials Engineering,
The University of Western Ontario, London,
ON N6A 5B8, Canada
e-mail: xsun@eng.uwo.ca

beginning of the twenty-first century, the applications of ALD have been widened into nanotechnology for synthesizing various novel nanostructures and nano-devices of different elements and compounds, as reviewed by Knez et al. (2007) and Kim et al. (2008a).

One of a variety of strategies to apply ALD in nanofabrication is to synthesize one-dimensional (1D) coaxial nanostructures, with exactly controlled size and versatile functions, by selecting 1D templates (e.g., nanotubes, nanowires, etc.). Potential applications of the 1D coaxial nanostructures have been recently addressed as well, e.g., $ZnO–Al_2O_3$ core–shell nanowires for field effect transistors (Huang et al. 2008; Yang et al. 2008a), $CuO–Al_2O_3$ core–shell nanowires and Cu nanoparticle chains encapsulated by Al_2O_3 nanotubes for plasmon wave-guides (Qin et al. 2008). Among the 1D templates for the aforementioned nanosynthesis via ALD, carbon nanotubes (CNTs) appear to be a good candidate and contribute to a large number of nanoscale coaxial structures (Farmer and Gordon 2005, 2006; Herrmann et al. 2005; Kim et al. 2008b; Lee et al. 2003; Ras et al. 2007; Zhan et al. 2008), which possess enhanced physical and chemical properties due to the coaxial combination of CNTs and the target coatings. However, because of their chemical inertness to ALD precursors and the surface-controlled nature of ALD (Leskelä and Ritala 2003; Ritala and Leskelä 1999), single-walled (SWCNTs) or multi-walled (MWCNTs) CNTs need surface functionalization through covalent or non-covalent chemical methods (Farmer and Gordon 2005, 2006; Zhan et al. 2008).

Iron(III) oxide (Fe_2O_3) as a transition metal oxide has drawn much attention from ALD due to its potential applications in photocatalysis, gas-sensing, and the magnetic fields. Depending on different templates, earlier studies have fulfilled the ALD of Fe_2O_3 (ALD-Fe_2O_3) with various nanostructures, such as Fe_2O_3 thin films on flat substrates (e.g., Si and glass wafers) (Aronniemi et al. 2008; Lie et al. 2005; Nilson et al. 2004; Rooth et al. 2008), Fe_2O_3 nanotubes via porous template-directed routes (Bachmann et al. 2007; Daub et al. 2007; Rooth et al. 2008), and Fe_2O_3 composites based on zirconia nanoparticles (Scheffe et al. 2009). The ALD precursors used in the aforementioned studies include $Fe(thd)_3$ and ozone (Lie et al. 2005; Nilson et al. 2004), $FeCl_3$ and water (Aronniemi et al. 2008),

ferrocene ($Fe(C_5H_5)_2$) and oxygen (Rooth et al. 2008; Scheffe et al. 2009), ferrocene and ozone (Daub et al. 2007), as well as $Fe_2(O^tBu)_6$ and water (Bachmann et al. 2007). However, there have been few efforts to date to synthesize 1D coaxial nanostructures of Fe_2O_3 using ALD. In order to explore the possibility of developing such 1D nanostructure via ALD, recently we attempted to deposit Fe_2O_3 on CNTs. As a consequence, as will be exposed in this article, heterostructural coaxial nanotubes via ALD coating of CNTs with Fe_2O_3 (i.e., CNT@Fe_2O_3) were developed with the precursors of ferrocene and oxygen. In this study, two types of CNTs, undoped and nitrogen-doped (N-doped), were employed as templates. It confirmed that functionalized pretreatment of the undoped CNTs is essential for ALD-Fe_2O_3, due to their inert surface nature. In contrast, it was demonstrated for the first time that N-doped CNTs (N-CNTs), ascribing to their chemically active surface nature, appeared as a more reliable alternative for tunable ALD-Fe_2O_3. As a consequence, besides the disclosure on the effects of different functionalization methodologies, this study opened a facile avenue to produce various heterostructural coaxial nanotubes of CNT@Fe_2O_3 using N-CNTs, which are expected to find great applications in producing functional components for various nanodevices.

Experimental

Synthesis and functionalization of CNTs

Synthesis

The two types of CNTs were synthesized by thermal CVD methods in a heated horizontal quartz tube. A series of carbon papers as substrates to grow CNTs were covered with 30 nm thick aluminum at the bottom and 5 nm thick iron at the top. In the presence of Ar, the undoped CNTs were grown through pyrolyzing ethylene (C_2H_4) at 750°C (Liu et al. 2008) while the N-CNTs were produced by pyrolyzing melamine ($C_3H_6N_6$) at 800°C (Zhong et al. 2010). They both are structurally multi-walled, but the N-CNTs received an N content of around 10.4 at.% determined by X-ray photoelectron spectroscopy (XPS, Kratos Axis Ultra Al(alpha)) (Zhong et al. 2010).

Functionalization

Owing to their chemical inertness, undoped CNTs were usually functionalized for various deposition processes. There are mainly two methodologies practiced in previous studies: covalent oxidation and non-covalent surface modification. In the former case, it has been fulfilled with many chemical solutions, including HNO_3, a mixture of 3:1 HNO_3/H_2SO_4, $KMnO_4$, and so on (Datsyuk et al. 2008; Hu et al. 2003; Park et al. 2006; Pumera et al. 2009; Wang et al. 2009; Xia et al. 2007; Yu et al. 1998; Zhang et al. 2003, 2009). In the latter case, it was preformed by many surfactants, such as sodium dodecyl sulfate (SDS), sodium dodecyl benzenesulfonate (SDBS), etc. (Huang et al. 2004; Islam et al. 2003; Rastogi et al. 2008; Tummala and Striolo 2009; Usrey and Strano 2009; Wanless and Ducker 1996; Zhang et al. 2006). Among them, HNO_3 and SDS are the most widely used ones as the covalent and non-covalent approach, respectively (Islam et al. 2003; Park et al. 2006).

For an aim of comparison, in this study we employed both covalent and non-covalent methods to modify the surface of undoped CNTs. In the case of covalent oxidation, samples of CNTs were soaked in a concentrated 70% HNO_3 solution at room temperature for 2 h, and then fully rinsed with deionized water (DI H_2O). In the case of non-covalent modification, samples were dipped into the aqueous solution of 1 wt% SDS [concentration greater than the critical micelle concentration (Wanless and Ducker 1996; Zhang et al. 2006)] at room temperature for 2 h. The 2-h treatment was beneficial in two ways: (1) protecting CNTs from cutting and damage due to extended chemical oxidation of HNO_3 or providing enough wetting to CNTs in the SDS surfactant; (2) facilitating to conduct a comparative study on different functionalization methods. In addition, the combined effects due to the two aforementioned functionalization methods were examined by treating CNTs with HNO_3 for 1 h, fully rinsing the oxidized samples, and then immersing the samples with SDS for 1 h.

ALD-Fe_2O_3 processes

With the samples of CNTs loaded in a commercial ALD reactor (Savannah 100, Cambridge Nanotechnology Inc., USA), ALD-Fe_2O_3 was performed with ferrocene and oxygen as precursors. Although the two precursors had their ALD successes reported previously on other templates (Rooth et al. 2008; Scheffe et al. 2009), there is still a bit of vague in exactly understanding the mechanisms. In general, it was postulated that this ALD-Fe_2O_3 consists of the two potential half-reactions (Scheffe et al. 2009): (1) ferrocene ligands react with chemisorbed oxygen in the ferrocene pulse, and (2) oxygen reacts with the remaining chemisorbed ferrocene ligands in the oxygen pulse. In this study, ferrocene (98%, Sigma-Aldrich) and oxygen (99.9%) were introduced into the ALD reactor in an alternating manner. Prior to the ALD-Fe_2O_3, ferrocene powder as the iron source was heated to 90°C. As a consequence, the partial pressures for ferrocene and oxygen were 10 and 400 Torr, respectively. Nitrogen was selected as the carrier gas with a flow rate of 20 sccm. The reactor was evacuated in ALD processes by a vacuum pump (Pascal 2005 I, Adixon), and reached a base pressure of around 0.4 Torr. The growth temperature of the substrates was set at 350°C, and the wall temperature of the reactor was 270°C. In detail, the ALD-Fe_2O_3 processes were composed of several steps: (1) a 3-s supply of ferrocene; (2) a 5-s extended exposure of ferrocene to CNTs; (3) a 25-s nitrogen purge to remove oversupplied ferrocene and possible by-products; (4) a 2-s supply of oxygen; (5) a 5-s extended exposure of oxygen to CNTs; (6) a 25-s nitrogen purge to remove oversupplied oxygen and possible by-products. A whole set of the aforementioned six steps constituted one ALD cycle, and ALD processes could differ in the number of cycles in this study. Compared with the previous studies (Rooth et al. 2008; Scheffe et al. 2009), this study applied a higher temperature (90°C) for preheating ferrocene. The growth temperature (350°C) was comparable to the lower ones employed in the literature (Rooth et al. 2008; Scheffe et al. 2009). In addition, the dosing of both ferrocene and oxygen in this study was longer than those used by Rooth et al. (2008) but shorter than the ones by Scheffe et al. (2009). In particular, an exposure mode with a longer purging was employed in this study.

Characterization techniques

A field-emission scanning electron microscope (FE-SEM, Hitachi 4800S) was employed to collect the

SEM images of the ALD-Fe$_2$O$_3$ on CNTs, showing the morphological changes of CNTs. Furthermore, the growth of the ALD-Fe$_2$O$_3$ was observed using a transmission electron microscope (TEM, Philips CM10). In addition, the crystalline structure of the ALD-Fe$_2$O$_3$ was examined by a high-resolution transmission electron microscope (HRTEM, JEOL 2010 FEG), and its composition was determined by a micro-X-ray diffractometer (XRD, Brucker D8).

Results and discussion

Effects of surface functionalization

The ALD-Fe$_2$O$_3$ was first performed on undoped CNTs. As for the pristine undoped CNTs, their morphological characteristics were shown in Fig. 1a, b jointly by low and high magnification SEM images. They were grown on carbon papers with high density and an average diameter in the range 20–60 nm. The conventional and high-resolution TEM images (Fig. 1c) further revealed their multiwalled structure.

To investigate the effects of surface modifications, a 200-cycle ALD-Fe$_2$O$_3$ was first practiced on the pristine undoped CNTs, as illustrated jointly by SEM image in Fig. 2a and TEM image in Fig. 2b. The two images, compared with Fig. 1b, c, revealed no

observable changes on the morphologies of the CNTs, indicating an unsuccessful ALD practice on the pristine undoped CNTs. The only reason lies in the structural perfectness of undoped CNTs (Balasubramanian and Burghard 2005; Wang et al. 2009), contributing to a chemically inert characteristic, for there were no active sites for ALD to bond precursor molecules. According to previous studies, in reality only some trace defects (1–3 at.%) were disclosed (Hu et al. 2001; Zhang et al. 2003). To promote the ALD-Fe$_2$O$_3$ on undoped CNTs, thus, we employed both covalent and non-covalent chemical methods to modify the surface nature of undoped CNTs and their effects were investigated.

The first attempt to promote the ALD-Fe$_2$O$_3$ was conducted by the pretreatment of undoped CNTs with HNO$_3$, and the effect is illustrated in Fig. 2c, d by SEM images. Obviously, this covalent oxidization method helped the growth of the ALD-Fe$_2$O$_3$ in some local regions of CNTs where iron oxide clusters were grown. The clusters ranged in sizes and morphologies from nanoparticles of several tens nanometers to patchy films of hundreds nanometers. In particular, some uncoated areas are easily observed on the CNTs. As an alternative, in comparison, another effort was carried out with a non-covalent surfactant, SDS, and its effect is shown in Fig. 2e, f by SEM images. It was found that the treatment of SDS

Fig. 1 The pristine undoped CNTs: **a** low magnification and **b** high magnification SEM image; **c** conventional and (*inset*) high-resolution TEM image
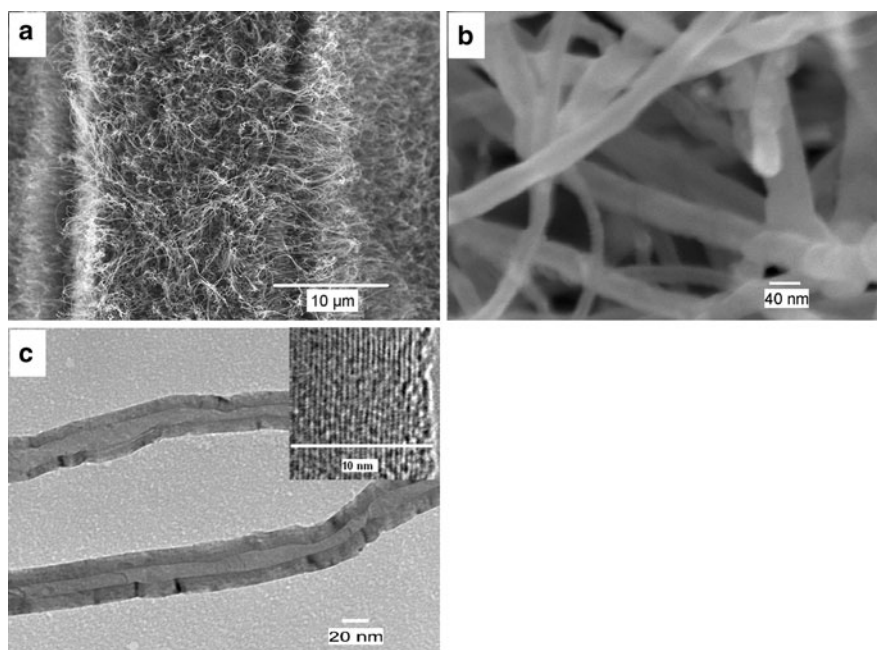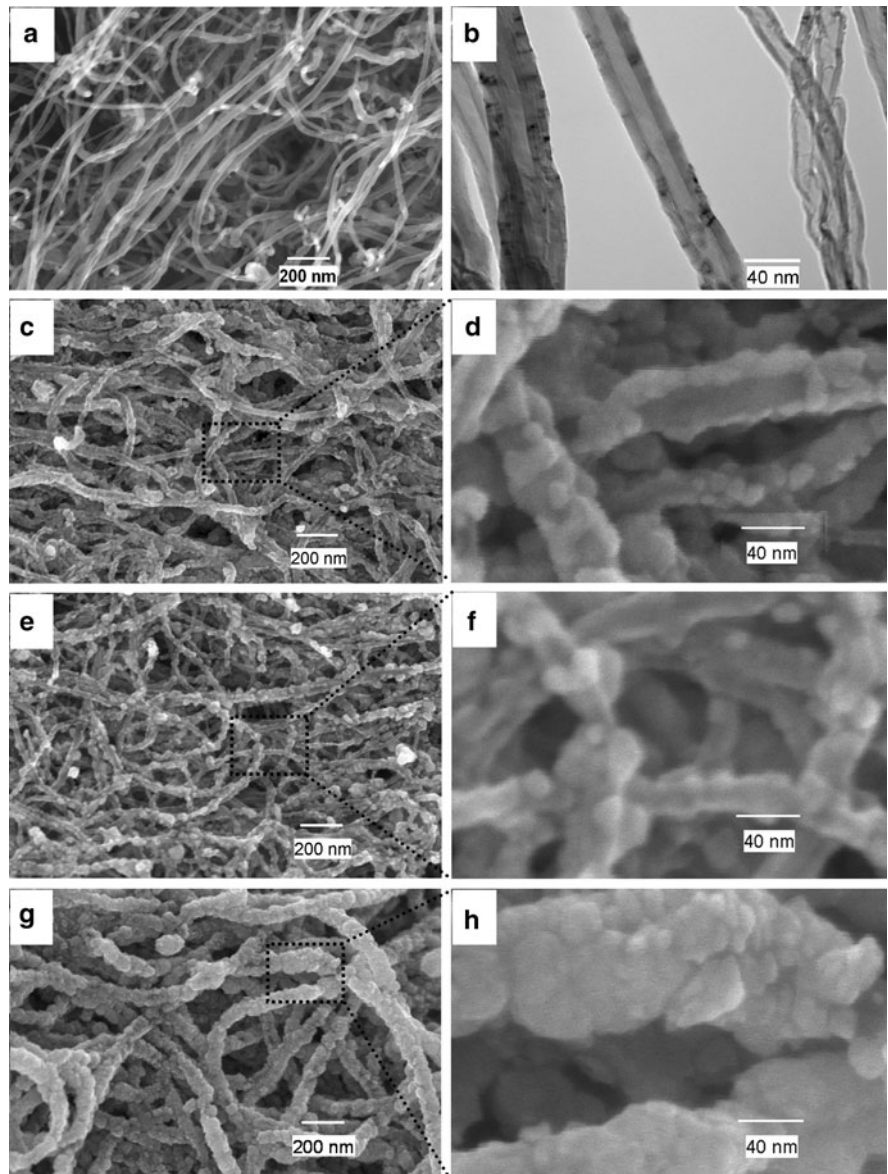
Fig. 2 200-cycle ALD of iron oxide deposition on the undoped CNTs: without surface pretreatment, **a** SEM image and **b** TEM image; treated by 2 h nitric acid, **c** low magnification and **d** high magnification SEM image; treated by 2 h SDS, **e** low magnification and **f** high magnification SEM image; treated by 1 h nitric acid and 1 h SDS in sequence, **g** low magnification and **h** high magnification SEM image

received a similar effect as the one of HNO_3: scattered clusters but not continuous film. Furthermore, we also examined the combined effect due to sequential HNO_3 and SDS treatment, as revealed by Fig. 2g, h. In this case, the CNTs were almost fully covered with a fairly thick film, resulting in an increase in diameters from 20–60 to 60–80 nm after 200 ALD cycles. However, it is still remarkable that the coverage is non-uniform. In addition, the coated samples due to HNO_3 treatment and due to SDS treatment were examined by XRD, illustrated in Fig. 3. The XRD patterns show two stronger peaks

identified as the reference values of crystalline graphite in the standard card (JCPDS PDF No. 41-1487). They should be caused by the templates and marked as Graphite(002) and Graphite(004). The other two weaker peaks, as marked as (110) and (104), were confirmed in the standard card (JCPDS PDF No. 33-0664) and contributed crystalline α-Fe_2O_3 (hematite) to be identified for both cases.

To understand the effects of the covalent and non-covalent functionalization on the ALD-Fe_2O_3, it is essential to know the knowledge of the changed surface nature. In the case of HNO_3 treatment,
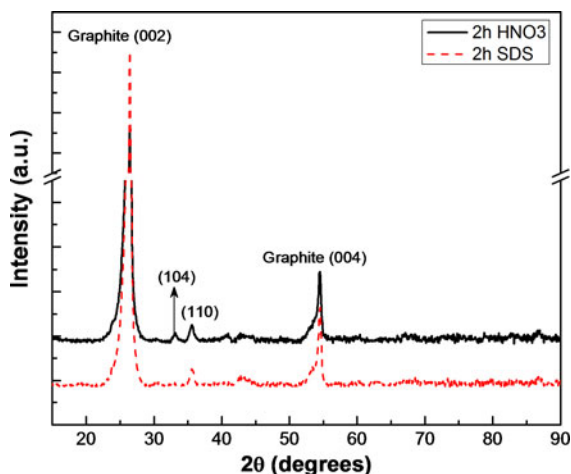
Fig. 3 XRD patterns of the ALD iron oxide on the undoped CNTs treated by nitric acid and SDS

extensive investigation conducted previously revealed that oxygenated functional groups (e.g., carboxylic (–COOH), hydroxyl (–OH), phenolic (–OH bonded to a phenyl ring (C_6H_5–)), etc.) were introduced to CNTs while metal catalysts and amorphous carbon were removed (Datsyuk et al. 2008; Hu et al. 2003; Park et al. 2006; Pumera et al. 2009; Wang et al. 2009; Xia et al. 2007; Zhang et al. 2003, 2009). Due to the various functional groups generated by acid oxidation, consequently, the surface reactivity of CNTs is significantly enhanced (Yu et al. 1998). A case study using microwave method (Kim et al. 2007) disclosed that the oxidized CNTs via HNO_3 promoted the growth of Pt nanoparticles, for the created oxygenated defects provided Pt atoms with large adsorption energy. In the case of the non-covalent SDS functionalization, its widespread use was mainly for dispersing CNTs but not changing their inherent properties (Huang et al. 2004; Islam et al. 2003; Rastogi et al. 2008; Usrey and Strano 2009; Zhang et al. 2006). Over a critical solution concentration, SDS molecules would aggregate in interfaces (Wanless and Ducker 1996). A recent simulation (Tummala and Striolo 2009) indicated that the morphologies and coverage of SDS aggregates have strong dependence on the diameter of CNTs, and get better with the increased diameter. In particular, the hydrophobic long-chain hydrocarbon tails of SDS molecules get adsorbed onto graphite surface by van der Waals attractions while their hydrophilic sulfate (SO_4^{2-}) head groups were

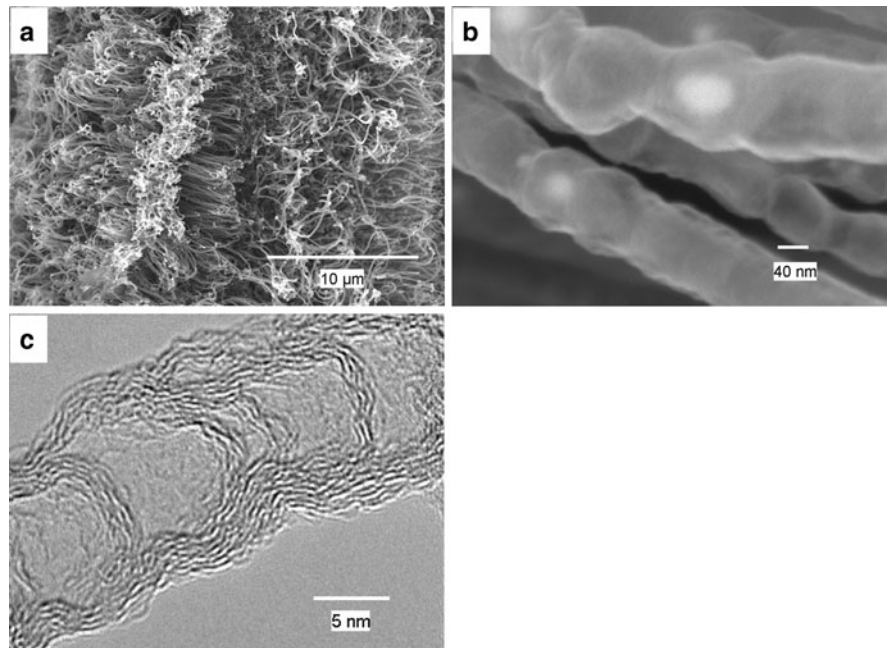exposed and served as ALD nucleation sites (Zhan et al. 2008).

Obviously, both HNO_3 and SDS treatment introduced functional groups to the surface of undoped CNTs and thereby changed their surface reactivity. As a consequence, the created functional groups served as active sites to initiate ALD-Fe_2O_3. In summary, the ALD-Fe_2O_3 on those modified CNTs can be explained with the mechanisms: (1) HNO_3 and/or SDS treatment created functional groups (oxygenated and/or sulfate groups) on the surface of undoped CNTs; (2) ferrocene ligands were partially oxidized by the created groups and thereby Fe chemisorbed on the surface of CNTs with some remaining ligands, indicating the initiation of ALD processes; (3) a following oxygen pulse oxidized the remaining ferrocene ligands with the product of iron(III) oxide as well as new functional groups for the next ferrocene pulse; and (4) the following cyclic ferrocene/oxygen pulses sustained the growth of crystalline Fe_2O_3.

As for the partial and non-uniform coverage on the CNTs treated by HNO_3 (Fig. 2c, d) or SDS (Fig. 2e, f), the reasons were mainly lied in the variances of CNTs in properties (such as perfectness, curvature, etc.), probably existing between individuals in a population of CNTs and/or regionally on a given CNT. Obviously, the functionalization effect due to HNO_3 or SDS was limited in each case. With reference to the improved coverage (Fig. 2g, h) due to the combined treatment of HNO_3 and SDS, there are two possibilities: (1) the initial oxidation-created defects improved the following SDS functionalization; (2) the sequential treatment by nitric acid and SDS produced a compensating effect on the creation of functional groups of CNTs. In any case of the two possibilities, there would be more active sites (in the forms of oxygenated or sulfate groups) to initiate the ALD-Fe_2O_3 by oxidizing ferrocene ligands in the first ferrocene pulse, leading to an improved coverage of Fe_2O_3 on the surface of CNTs.

Effects of N-doping

The above results disclosed an unsuccessful ALD-Fe_2O_3 on pristine undoped CNTs due to their structural perfectness, and an arbitrary ALD-Fe_2O_3 on undoped CNTs modified by HNO_3 and/or SDS. In order to synthesize 1D coaxial nanotubes of

Fig. 4 The N-doped CNTs:
a low magnification and
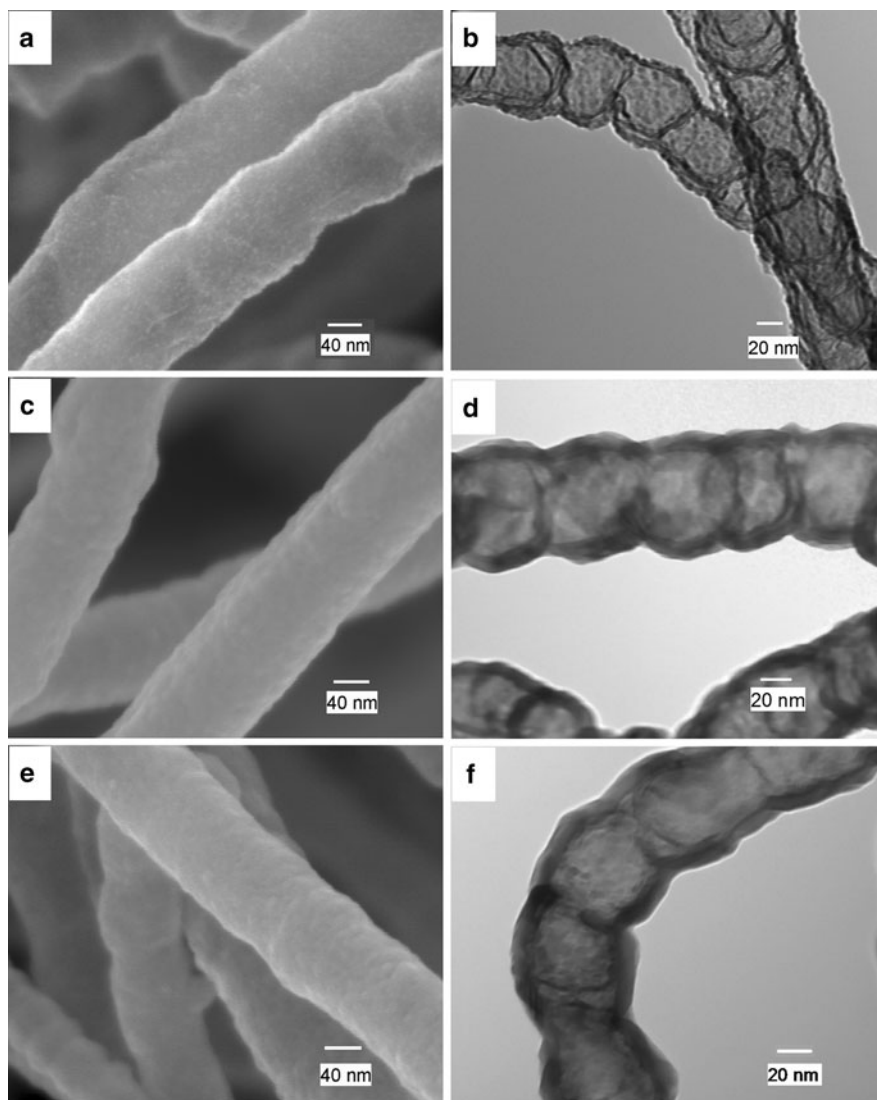**b** high magnification SEM
image; **c** HRTEM image

$CNT@Fe_2O_3$, we have to better manipulate ALD-Fe_2O_3. Fortunately, N-CNTs were found in this study to serve for this objective, and ALD-Fe_2O_3 was performed on N-CNTs under the same conditions as the ones for undoped CNTs. As shown in Fig. 4a, the N-CNTs were also grown on carbon papers with high density. They are morphologically bamboo-like and typically in the range 40–80 nm in diameter (Fig. 4b). HRTEM image (Fig. 4c) also revealed that they are multiwalled in structure.

In sharp contrast to the ALD-Fe_2O_3 on the pristine undoped CNTs (illustrated by Fig. 2a, b), the practice of ALD-Fe_2O_3 on the pristine N-CNTs exhibited some distinct characteristics. After 50 ALD cycles, as jointly shown by the SEM and TEM images in Fig. 5a, b, respectively, numerous nanoparticles of less than 5 nm were uniformly deposited on the N-CNTs. Furthermore, the TEM image (Fig. 5b) also revealed that a continuous but bumpy thin film has been formed by those tiny nanoparticles. In this case, a nanostructure of $CNT@Fe_2O_3$ nanoparticles was received. With the ALD increased to 70 (Fig. 5c, d) and 100 cycles (Fig. 5e, f), it was found that smooth and uniform films were formed on the N-CNTs, resulting in heterostructural coaxial nanotubes of $CNT@Fe_2O_3$. Remarkably, the growth of ALD-Fe_2O_3 on N-CNTs experienced two distinct stages: island-like (in the first 50 cycles) and 2D growth

mode (after 70 cycles). In addition, the film thickness was around 7.7 nm for 70 cycles and 11 nm for 100 cycles, accounting for a nearly linear growth rate of 1.1 Å/cycle on the N-CNTs. In addition, the examinations of XRD and HRTEM were conducted on the samples with a 70-cycle ALD-Fe_2O_3. In Fig. 6a, the XRD patterns disclosed that, besides the strong peaks of Graphite(002) and Graphite(004) (PCPDS PDF No. 41-1487) due to the crystalline graphite of the templates, the peaks of (110) and (104) were induced by α-Fe_2O_3 (hematite) (JCPDS PDF No. 33-0664) deposited via ALD. The HRTEM images in Fig. 6b, c demonstrated a single crystalline structure of as-deposited Fe_2O_3 as well as a 7.7-nm thick film. The measured lattice fringe spacing is 0.27 nm, indicating that the as-deposited Fe_2O_3 grew along a direction parallel to [110]. In comparison with the results exposed in previous studies, the growth rate of 1.1 Å/cycle in this study is a bit lower than the one [1.4 Å/cycle (Rooth et al. 2008)] on Si substrates but higher than the one [0.6 Å/cycle (Rooth et al. 2008)] in AAO pores and the one [0.15 Å/cycle (Scheffe et al. 2009)] on zirconia nanoparticles. In particular, different from the crystalline structures received in the study conducted by Rooth et al. (2008) and by us in this study, amorphous iron oxide was deposited on zirconia nanoparticles by Scheffe et al. (2009). All these aforementioned variances on film growth imply

Fig. 5 The ALD iron oxide on N-doped CNTs illustrated by: SEM images **a** 50 cycles, **c** 70 cycles, and **e** 100 cycles; TEM images **b** 50 cycles, **d** 70 cycles, and **f** 100 cycles
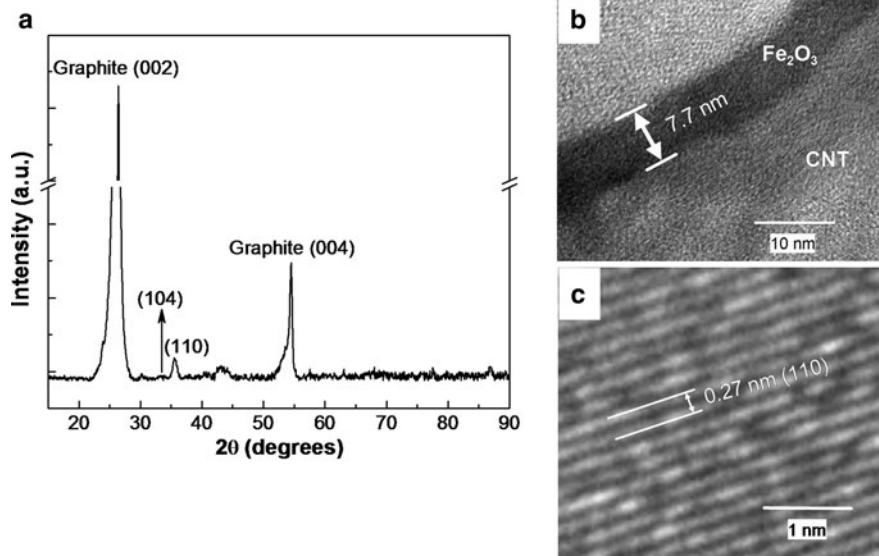

that experimental conditions, especially the nature of the employed templates, played important roles in determining the characteristics of film growth, such as growth rates and structural phases.

Obviously, the above-discussed results demonstrated that the N-CNTs behaved favorable for ALD-Fe$_2$O$_3$, implying that N-doping played an important role. The underlying mechanisms should be ascribed to the chemically active surface of N-CNTs induced by the intrinsically incorporated N atoms. According to earlier studies (Ewels and Glerup 2005; van Dommele et al. 2008; Yang et al. 2007, 2008b), the doped-N atoms contributed to a variety of N-related defects. Of them, two primary N-bonding configurations were extensively identified, i.e., graphite-like N (GN, in which an N atom replaces a graphitic C atom) and pyridine-like N (PN, in which an N atom is bonded with two C atoms). It was previously revealed that both the GN and PN atoms are responsible for the enhancement of the reactivity of N-CNTs, in spite of different underlying mechanisms associated with them (Ewels and Glerup 2005; Peng and Cho 2003; Stafström 2000). The former one results in N-neighboring C atoms activated, while the latter one contributes non-bonding electrons (Li et al. 2009; Yang et al. 2007). In practice, both experiments and simulations commonly demonstrated that N-CNTs promoted the deposition of transition metals

Fig. 6 Phase and composition characteristics of the ALD iron oxide (70 ALD cycles) on the N-doped CNTs: **a** XRD patterns, **b** TEM image, and **c** HRTEM image

and the PN tends to provide a higher binding energy in comparison to the one by GN (Li et al. 2009; Sun et al. 2009; Yang et al. 2007).

Based on the above discussion, it is reasonable to believe that in this study the doped-N atoms (no matter which bonding configuration was taken) have facilitated or promoted the adsorption of the molecules of the employed precursors onto the N-CNTs to initiate ALD-Fe_2O_3. As revealed in our previous study (Zhong et al. 2010), the N-CNTs employed in this study were with an N content of 10.4 at.%, and the area composition was 30.2% for GN and 54.6% for PN. On the other hand, the surface-controlled ALD determined that only the chemisorption between precursor molecules and functional groups is valid for the initiation of an ALD process (Puurunen 2005). Thus, one of the precursors (ferrocene and oxygen) must have been chemically adsorbed on N-CNTs at the beginning of ALD. The most recent study (Hu et al. 2010) revealed that oxygen can chemically adsorb on N-CNTs, but can only physically adsorb on undoped CNTs. Thus, the chemisorbed oxygen is one solution for the success of ALD-Fe_2O_3 on N-CNTs. On the other hand, previous successes of transition metals (Ni, Pt) on N-CNTs seem to imply another possibility for the initiation of ALD-Fe_2O_3, i.e., ferrocene might be able to chemically bond with the surface active sites of the N-CNTs. As for this postulation, there was still a lack in understanding. In any case, the doped-N provided the base for the

successful ALD-Fe_2O_3 on N-CNTs. After the initiation, the cyclic ferrocene/oxygen pulses sustained the growth of ALD-Fe_2O_3, having less direct interactions with the surface of N-CNTs.

To understand the growth characteristics of Fe_2O_3 on N-CNTs with ALD cycles, there are two main factors identified previously: the steric hindrance of precursors and the limited number of reactive sites (Kim et al. 2008a; Leskelä and Ritala 1995; Puurunen 2005; Ylilammi 1996). In the case of this study using ferrocene and oxygen as precursor, it is believed that the N content played an important role influencing the growth of Fe_2O_3. As shown in Fig. 5b, d, and f, there exists a transition from an island-like growth mode to a 2D film growth mode in the range 50–70 cycles, likely incurred by the limited number of reactive sites if not by steric hindrance. Recently, experimental investigation based on a solution method (Chen et al. 2009) demonstrated that higher N content resulted in smaller platinum particles with higher density deposited on N-CNTs. Therefore, we postulate that higher N content may increase the growth rate of the ALD-Fe_2O_3 and reduce the number of ALD cycles for the formation of coaxial Fe_2O_3 films on N-CNTs. In this way, a systematic investigation is of great interest in the future. In this study, it is worth noting that various coaxial nanotubes of CNT@Fe_2O_3 were synthesized using N-CNTs, and particularly Fe_2O_3 can be in the form of nanoparticles or films with well-controlled growth through adjusting the ALD cycles. In addition,

N-CNTs were free of any surface modification [which influence the properties of undoped CNTs more or less (Zhang et al. 2003; Zhao et al. 2004)] prior to ALD-Fe_2O_3 and thereby could sustain their inherent properties. More importantly, N-CNTs could be tailored in properties by tuning the doped-N and were demonstrated with improved properties, such as electrical conductivity (Nxumalo and Coville 2010). Thus, N-doping would contribute two important characteristics of the coaxial CNT@Fe_2O_3 nanotubes: (1) tunable deposition of ALD-Fe_2O_3; (2) tunable properties of N-CNTs. The two advantages would jointly lead to tunable functionality of the CNT@Fe_2O_3 nanodevices for gas-sensing, magnetic, and photocatalytic applications.

Conclusions

In this study, we attempted to synthesize 1D heterostructural coaxial nanotubes of CNT@Fe_2O_3 via atomic layer deposition using ferrocene and oxygen as precursors. It was found that, of the employed undoped and N-doped CNTs, the undoped ones needed chemical functionalization prior to ALD-Fe_2O_3, due to their inert surface nature. Even so, the functionalized undoped CNTs by HNO_3 or/and SDS were only coated with Fe_2O_3 in an arbitrary means, i.e., the as-deposited Fe_2O_3 was random and non-uniform. In sharp comparison, N-CNTs were more favorable for a uniform and tunable ALD-Fe_2O_3, ascribed to their chemically active surface nature induced by intrinsically incorporated N atoms. As a consequence, this study successfully fabricated 1D heterostructural nanotubes of CNT@Fe_2O_3 with tunable Fe_2O_3 from nanoparticles to nanofilms, based on N-CNTs. In addition, it was disclosed that the as-deposited Fe_2O_3 on the N-CNTs shows single-phase crystalline α-Fe_2O_3 (hematite), jointly determined by XRD and HRTEM. Essentially, this study provided an avenue for synthesizing 1D core–shell nanostructures using N-CNT as well as various heterostructural coaxial nanotubes of CNT@Fe_2O_3 being important candidates in many promising applications, such as photocatalysis, gas-sensing, magnetic fields, and other nanodevice fields.

References

Aronniemi M, Saino J, Lahtinen J (2008) Characterization and gas-sensing behavior of an iron oxide film prepared by atomic layer deposition. Thin Solid Films 516:6110–6115

Bachmann J, Jing J, Knez M, Barth S, Shen H, Mathur S, Gösele U, Nielsch K (2007) Ordered iron oxide nanotube arrays of controlled geometry and tunable magnetism by atomic layer deposition. J Am Chem Soc 129:9554–9555

Balasubramanian K, Burghard M (2005) Chemically functionalized carbon nanotubes. Small 1:180–192

Chen Y, Wang J, Liu H, Li R, Sun X, Ye S, Knights S (2009) Enhanced stability of Pt electrocatalysts by nitrogen doping in CNTs for PEM fuel cells. Electrochem Commun 11:2071–2076

Datsyuk V, Kalyva M, Papagelis K, Parthenios J, Tasis D, Siokou A, Kallitsis I, Galiotis C (2008) Chemical oxidation of multiwalled carbon nanotubes. Carbon 46:833–840

Daub M, Bachmann J, Jing J, Knez M, Gösele U, Barth S, Mathur S, Escirg J, Altbir D, Nielsch K (2007) Ferromagnetic nanostructures by atomic layer deposition: from thin films towards core–shell nanotubes. ECS Trans 11:139–148

Ewels CP, Glerup M (2005) Nitrogen doping in carbon nanotubes. J Nanosci Nanotech 5:1345–1363

Farmer DB, Gordon RG (2005) ALD of high-k dielectrics on suspended functionalized SWNTs. Electrochem Solid-State Lett 8:G89–G91

Farmer DB, Gordon RG (2006) Atomic layer deposition on suspended single-walled carbon nanotubes via gas-phase noncovalent functionalization. Nano Lett 6:699–703

Groner MD, Fabreguette FH, Elam JW, George SM (2004) Low-temperature Al_2O_3 atomic layer deposition. Chem Mater 16:639–645

Herrmann CF, Fabreguette FH, Finch DS, Geiss R, George SM (2005) Multilayer and functional coatings on carbon nanotubes using atomic layer deposition. Appl Phys Lett 87:123110

Hu H, Bhowmik P, Zhao B, Hamon MA, Itkis ME, Haddon RC (2001) Determination of the acidic sites of purified single-walled carbon nanotubes by acid-base titration. Chem Phys Lett 345:25–28

Hu H, Zhao B, Itkis ME, Haddon RC (2003) Nitric acid purification of single-walled carbon nanotubes. J Phys Chem B 107:13838–13842

Hu X, Wu Y, Li H, Zhang Z (2010) Adsorption and activation of O_2 on nitrogen-doped carbon nanotubes. J Phys Chem C 114:9603–9607

Huang L, Cui X, Dukovic G, O'Brien SP (2004) Self-organizing high-density single-walled carbon nanotube arrays from surfactant suspensions. Nanotechnology 15:1450–1454

Huang J, Liu S, Wang Y, Ye Z (2008) Fabrication of ZnO/Al$_2$O$_3$ core-shell nanostructures and crystalline nanotube. Appl Surf Sci 254:5917–5920

Islam MF, Rojas E, Bergey DM, Johnson AT, Yodh AG (2003) High weight fraction surfactant solubilization of single-wall carbon nanotubes in water. Nano Lett 3:269–273

Kim H (2003) Atomic layer deposition of metal and nitride thin films: current research efforts and applications for semiconductor device processing. J Vac Sci Technol B 21:2231–2261

Kim SJ, Park YJ, Ra EJ, Kim KK, An KH, Lee YH, Choi JY, Park CH, Doo SK, Park MH, Yang CW (2007) Defect-induced loading of Pt nanoparticles on carbon nanotubes. Appl Phys Lett 90:023114

Kim H, Lee HBR, Maeng WJ (2008a) Application of atomic layer deposition to nanofabrication and emerging nanodevices. Thin Solid Films 517:2563–2580

Kim DS, Lee SM, Scholz R, Knez M, Gösele U, Fallert J, Kalt H, Zacharias M (2008b) Synthesis and optical properties of ZnO and carbon nanotube based coaxial heterostructures. Appl Phys Lett 93:103108

Knez M, Nielsch K, Niinistö L (2007) Synthesis and surface engineering of complex nanostructures by atomic layer deposition. Adv Mater 19:3425–3438

Lee JS, Min B, Cho K, Kim S, Park J, Lee YT, Kim NS, Lee MS, Park SO, Moon JT (2003) Al$_2$O$_3$ nanotubes and nanorods fabricated by coating and filling carbon nanotubes with atomic-layer deposition. J Cryst Growth 254:443–448

Leskelä M, Ritala M (1995) Atomic layer epitaxy in deposition of various oxide and nitride. J Phys IV C5:937–951

Leskelä M, Ritala M (2003) Atomic layer deposition chemistry: recent development and future challenges. Angew Chem Int Ed 42:5548–5554

Li YH, Hung TH, Chen CW (2009) A first-principles study of nitrogen- and boron-assisted platinum adsorption on carbon nanotubes. Carbon 47:850–855

Lie M, Fjellvag H, Kjekshus A (2005) Growth of Fe$_2$O$_3$ thin films by atomic layer deposition. Thin Solid Films 488:74–81

Liu H, Arato D, Li R, Zhang Y, Merel P, Sun X (2008) Aligned multi-walled carbon nanotubes on different substrates by floating catalyst chemical vapor deposition: critical effects of buffer layer. Surf Coating Tech 202:4114–4120

Nilson O, Lie M, Foss S, Fjellvag H, Kjekshus A (2004) Effect of magnetic field on the growth of α-Fe$_2$O$_3$ thin films by atomic layer deposition. Appl Surf Sci 227:40–47

Nxumalo EN, Coville NJ (2010) Nitrogen doped carbon nanotubes from organometallic compounds: a review. Materials 3:2141–2171

Park TJ, Banerjee S, Hemraj-Benny T, Wong SS (2006) Purification strategies and purity visualization techniques for single-walled carbon nanotubes. J Mater Chem 16:141–154

Peng S, Cho K (2003) Ab Initio study of doped carbon nanotube sensors. Nano Lett 3:513–517

Pumera M, Šmid B, Veltruská K (2009) Influence of nitric acid treatment of carbon nanotubes on their physico-chemical properties. J Nanosic Nanotechnol 9:2671–2676

Puurunen RL (2005) Surface chemistry of atomic layer deposition: a case study for the trimethylaluminum/water process. J Appl Phys 97:121301

Qin Y, Lee SM, Pan A, Gösele U, Knez M (2008) Rayleigh-instability-induced metal nanoparticle chains encapsulated in nanotubes produced by atomic layer deposition. Nano Lett 8:114–118

Ras RHA, Kemell M, de Wit J, Ritala M, ten Brinke G, Leskelä M, Ikkala O (2007) Hollow inorganic nanospheres and nanotubes with tunable wall thickness by atomic layer deposition on self-assembled polymeric templates. Adv Mater 19:102–106

Rastogi R, Kaushal R, Tripathi SK, Sharma AL, Kaur I, Bharadwaj LM (2008) Comparative study of carbon nanotube dispersion using surfactants. J Colloid Interface Sci 328:421–428

Ritala M, Leskelä M (1999) Atomic layer epitaxy—a valuable tool for nanotechnology? Nanotechnology 10:19–24

Rooth M, Johansson A, Kukli K, Aarik J, Boman M, Hazrsta A (2008) Atomic layer deposition of iron oxide thin films and nanotubes using ferrocene and oxygen as precursors. Chem Vap Deposition 14:67–70

Scheffe JR, Francés A, King DM, Liang X, Branch BA, Cavanagh AS, George SM, Weimer AW (2009) Atomic layer deposition of iron (III) oxide on zirconia nanoparticles in a fluidized bed reactor using ferrocene and oxygen. Thin Solid Films 517:1874–1879

Stafström S (2000) Reactivity of curved and planar carbon-nitride structures. Appl Phys Lett 77:3941–3943

Sun S, Zhang G, Zhong Y, Liu H, Li R, Zhou X, Sun X (2009) Ultrathin single crystal Pt nanowires grown on N-doped carbon nanotubes. Chem Commun 45:7048–7050

Suntola T (1989) Atomic layer epitaxy. Mater Sci Rep 4:261–312

Suntola T and Antson J (1977) Method for producing compound thin films. US Patent 4058430

Tummala NR, Striolo A (2009) SDS surfactants on carbon nanotubes: aggregate morphology. ACS Nano 3:595–602

Usrey ML, Strano MS (2009) Controlling single-walled nanotubes surface adsorption with covalent and noncovalent functionalization. J Phys Chem C 113:12443–12453

van Dommele S, Romero-Izquirdo A, Brydson R, de Jong KP, Bitter JH (2008) Tuning nitrogen functionalities in catalytically grown nitrogen-containing carbon nanotubes. Carbon 46:138–148

van Hemmen JL, Heil SBS, Klootwijk JH, Roozeboom F, Hodson CJ, van de Sanden MCM, Kessels WMM (2007) Plasma and thermal ALD of Al$_2$O$_3$ in a commercial 200 mm ALD reactor. J Electrochem Soc 154:G165–G169

Wang Z, Shirley MD, Meikle ST, Whitby RLD, Mikhalovsky SV (2009) The surface acidity of acid oxidized multi-walled carbon nanotubes and the influence of in situ generated fulvic acids on their stability in aqueous dispersions. Carbon 47:73–79

Wanless EJ, Ducker WA (1996) Organization of sodium dodecyl sulfate at the graphite-solution interface. J Phys Chem 100:3207–3214

Xia W, Wang Y, Bergsträßer R, Kundu S, Muhler M (2007) Surface characterization of oxygen-functionalized multi-walled carbon nanotubes by high-resolution X-ray photoelectron spectroscopy and temperature-programmed desorption. Appl Surf Sci 254:247–250

Yang SH, Shin WH, Lee JW, Kim HS, Kang JK, Kim YK (2007) Nitrogen-mediated fabrication of transition metal-

carbon nanotube hybrid materials. Appl Phys Lett 90:013103

Yang Y, Kim DS, Knez M, Scholz R, Berger A, Pippel E, Hesse D, Gösele U, Zacharias M (2008a) Influence of temperature on evolution of coaxial ZnO/Al$_2$O$_3$ one-dimensional heterostructures: from core-shell nanowires to spinel nanotubes and porous nanowires. J Phys Chem C 112:4068–4074

Yang SH, Shin WH, Kang JK (2008b) The nature of graphite- and pyridine-like nitrogen configuration in carbon nitride nanotubes: dependence on diameter and helicity. Small 4:437–441

Ylilammi M (1996) Monolayer thickness in atomic layer deposition. Thin Solid Films 279:124–130

Yu R, Chen L, Liu Q, Lin J, Tan KL, Ng SC, Chan HSO, Xu GQ, Andy Hor TS (1998) Platinum deposition on carbon nanotubes via chemical modification. Chem Mater 10:718–722

Zhan GD, Du X, King DM, Hakim LF, Liang X, McCormick JA, Weimer AW (2008) Atomic layer deposition on bulk quantities of surfactant-modified single-walled carbon nanotubes. J Am Ceram Soc 91:831–835

Zhang J, Zou H, Qing Q, Yang Y, Li Q, Liu Z, Guo X, Du Z (2003) Effect of chemical oxidation on the structure of single-walled carbon nanotubes. J Phys Chem B 107:3712–3718

Zhang M, Su L, Mao L (2006) Surfactant functionalization of carbon nanotubes (CNTs) for layer-by- layer assembling of CNT multi-layer films and fabrication of gold nano-particles/CNT nanohybrid. Carbon 44:276–283

Zhang ZB, Li J, Cabezas AL, Zhang SL (2009) Characterization of acid-treated carbon nanotube thin films by means of Raman spectroscopy and field-effect response. Chem Phys Lett 476:258–261

Zhao J, Park H, Han J, Lu JP (2004) Electronic properties of carbon nanotubes with covalent sidewall functionalization. J Phys Chem B 108:4227–4230

Zhong Y, Jaidann M, Zhang Y, Zhang G, Liu H, Ionescua MI, Li R, Sun X, Abou-Rachid H, Lussierb LS (2010) Synthesis of high nitrogen doping of carbon nanotubes and modeling the stabilization of filled DAATO@CNTs (10, 10) for nanoenergetic materials. J Phys Chem Solids 71:134–139